Quantitative analysis of BMP-2 derived peptide covalently grafted onto oxidized detonation nanodiamonds

Sascha Balakin[a,b], Athanassios Missirlis[b], Benjamin Klemmed[c], Jihye Lee[d], Jörg Opitz[a,b,*], Jong-Souk Yeo[d] and Gianaurelio Cuniberti[a,*]

a Institute for Materials Science and Max Bergmann Center of Biomaterials, Technische Universität Dresden, 01062 Dresden, Germany
b Fraunhofer Institute for Ceramic Technologies and Systems IKTS Material Diagnostics, 01109 Dresden, Germany
c Physical Chemistry, Technische Universität Dresden, 01062 Dresden, Germany
d School of Integrated Technology, Yonsei University, Incheon 406-840, Republic of Korea

*Corresponding authors. Tel.: +49 351 88815516. E-mail: Joerg.opitz@ikts.fraunhofer.de (Jörg Opitz). Tel.: +49 351 46331420. E-mail: gianaurelio.cuniberti@tu-dresden.de (Gianaurelio Cuniberti)

Formal publication via DOI: https://doi.org/10.1016/j.carbon.2019.05.064

Abstract

In order to deploy detonation nanodiamonds (NDs) in nanomedicine and drug delivery applications, fundamental understanding of their surface chemistry and drug loading capacity is highly desirable. Herein, bone morphogenetic protein 2 (BMP-2) derived peptide with the sequence *KIPKASSVPTELSAISTLYLGGC* (molecular weight = 2336 g/mol) have been successfully grafted onto NDs using carbodiimide crosslinker chemistry. Initially, functional surface groups of wet- and dry-oxidized NDs were compared using infrared and mass spectroscopy. Dry-oxidized NDs exhibited the highest amount of carboxylic acid derivatives with a surface loading of 0.113 mmol/g after air annealing at 415 °C for 5 hours as determined by mass spectroscopy. Compared to wet-oxidation, the dry-oxidation process showed a 1.4-fold increased amount of carbonyl compounds deduced from infrared and mass spectroscopy. Crosslinking of the carboxylic acid derivatives to the primary amines of BMP-2 derived peptide is feasible in the range of 30-96% total surface coverage of NDs. 1:1 and 5:1 ND-peptide ratios

were utilized to study the surface loading of NDs using fluorescence spectroscopy. The chemisorption of BMP-2 derived peptide onto NDs reveals superior surface coverage and results in reproducible amounts of tethered bioactive molecules.

Graphical abstract

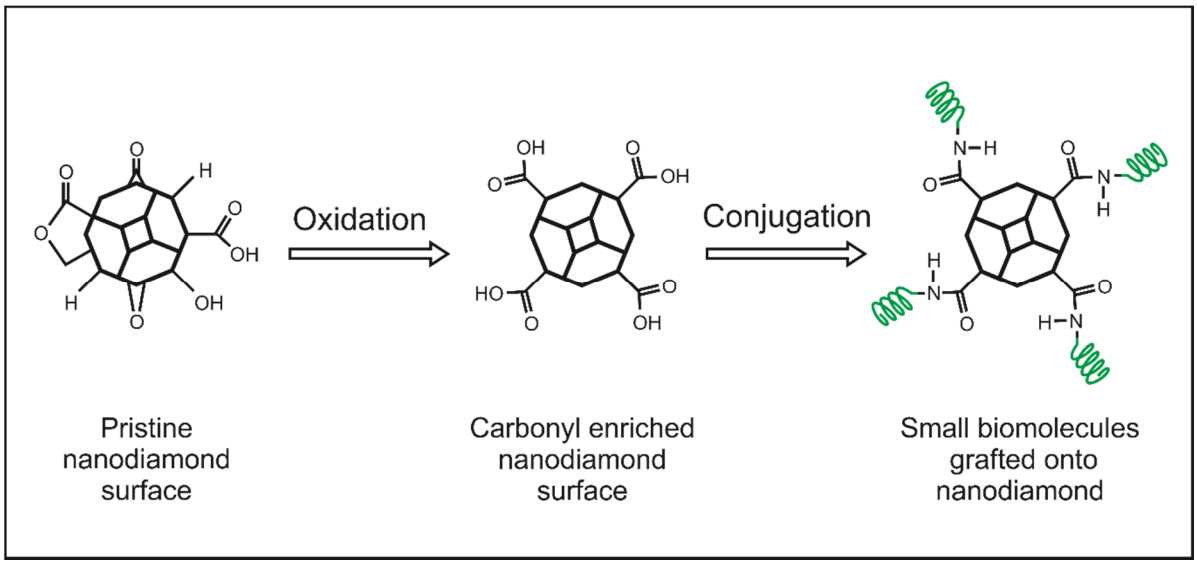

1. Introduction

Detonation nanodiamonds (NDs) are an emerging class of carbon-based nanoparticles. Due to their unique properties, such as a rich surface chemistry, high biocompatibility and resistance to harsh environments NDs are used in a broad range of interdisciplinary research areas [1,2,3,4]. Recently, ND research has led to bio-imaging, biosensing, drug and gene delivery applications for regenerative and personalized medicine [5,6,7,8,9]. NDs conjugated to antimicrobial agents are promising composite biomaterials for root canal therapy [10]. NDs as small interfering ribonucleic acid (siRNA) gene delivery vehicles showed a selective gene silencing effect in carcinoma cells, which enables an effective cancer treatment [11]. Furthermore, it has been shown that NDs are capable of dual functionalization for multimodal imaging and mitochondrial targeting. Those dually functionalized NDs are used to specifically target overexpressed folate receptors in cancer cells and to alter the intercellular localization to mitochondria [12]. In order to modulate the osteogenic differentiation of stem cells, NDs have been conjugated to the steroid dexamethasone as drug delivery vehicles [13].

The conjugation of NDs with growth factors for bone tissue engineering is a potential pathway to promote bone healing and to modulate the basic multicellular unit. Growth factors are

particularly interesting due to their ability to regulate a variety of cellular processes and to trigger tissue regeneration [14]. ND suspensions showed the capability of simultaneous delivery of two physisorbed proteins, bone morphogenetic protein 2 (BMP-2) and basic fibroblast growth factor (bFGF) to promote bone formation [15]. Li *et al.* showed an increased cell adhesion and viability of osteoblasts on hydroxyapatite coatings in combination of BMP-2 physisorbed onto NDs [16]. Although 20 different BMPs have been discovered, only BMP-2 is currently FDA approved and available in recombinant form for use in human spine surgery [17]. However, serious concerns have been raised regarding many adverse effects caused by excessive concentrations of BMP-2. Side effects include ectopic bone formation, inflammatory complications and possible tumour formation [18]. It has been demonstrated, that overexpression of BMP-2 in nasopharyngeal carcinoma cells promoted cell proliferation, migration, invasiveness and epithelial-mesenchymal transition [19]. High doses over 40 mg BMP-2 in lumbar spinal arthrodesis were associated with an increased risk of cancer [20]. Therefore, new pathways to use BMP-2 effectively have to be developed [21]. Regulation of BMP-2 dosage, sufficient drug delivery vehicles, and localization at the defect site are crucial factors for the successful implementation of BMP-2 [22]. Tailored drug delivery vehicles of BMP-2 derived peptides are promising candidates to overcome the above discussed disadvantages. The derived peptide can be synthetically produced and are more resistant to denaturation due to its smaller size and lower structural complexity. Additionally, short polypeptides show no immunogenicity compared to proteins [23].

This work describes the extension of the established covalent conjugation of NDs [24,25] by using BMP-2 derived osteogenic peptide. The pathway of conjugation includes the oxidization of NDs and application of zero-length crosslinking agents. As-received and dry-oxidized ND agglomerates with an initial mean hydrodynamic diameter of 26±2 nm and 34±5 nm were used to bind osteogenic peptide. This study focuses on the quantification of functional surface groups and the analysis of the surface loading capability of NDs with respect to future drug delivery applications. Our report leads to a better understanding regarding the controlled covalent binding of BMP-2 derived peptide and paves the way to tailored ND growth factor delivery vehicles.

2. Experimental procedure

2.1 Materials and reagents

Detonation nanodiamonds (NDs) were purchased from PlasmaChem GmbH, Berlin, Germany. The declared average particle size is 4 nm. The BMP-2 derived peptide sequence

(KIPKASSVPTELSAISTLYLGGC) was found to bind to both BMPrI and BMPrII receptors [26] and was ordered from Biotrend Chemikalien GmbH, Köln, Germany. 1-ethyl-3-(3-dimethylaminopropyl)carbodiimide (EDC) was obtained from Carl Roth GmbH Co. KG, Karlsruhe, Germany. N-Hydroxysuccinimide (NHS), 2-mercaptoethanol, and all other reagents used in this work were purchased from Merck KGaA, Darmstadt, Germany. Type 1 ultrapure water (ddH_2O) was collected using a Direct-Q 3 UV System water purifier by Merck KGaA, Darmstadt, Germany.

2.2 De-agglomeration and oxidation pathways of NDs

In order to homogenize aqueous ND suspensions, bead-milling was applied. In brief, 0.75 g of as-received NDs were suspended in 15 mL of double-distilled water (ddH_2O) along with 7.5 g of 100 µm ZrO_2 beads by Sigmund Linder GmbH, Warmensteinach, Germany. The milling treatment consisted of two consecutive cycles (700 rpm for 30 min) using the planetary micro mill Pulverisette 7 by Fritsch GmbH, Idar-Oberstein, Germany. Further de-agglomeration steps utilized ultrasound treatments. The pH-value of ND suspensions were adjusted to pH = 9 using 75 mM NaOH. Subsequently, the aqueous ND suspensions were subjected to 30 min of ultrasound treatment. The applied oscillation frequency of the submerged ultrasound probe was 20 kHz at 70% of the instrument's power output operated on the pulsed cycle with a 0.7 s active and 0.3 s passive intervals using a Sonopuls HD 2200 ultrasonic homogenizer by Bandelin electronic GmbH and Co. KG, Berlin, Germany.

The wet oxidation pathway of NDs utilizing a mixture of H_2SO_4:HNO_3 (9:1) was performed according to the protocol of Jee *et al.* [27]. The dry oxidation of NDs was performed using air annealing at 415 °C (heating rate of 20 K/min) for 5 h in a high temperature furnace from Thermconcept GmbH (model HTK 16/17), Bremen, Germany.

2.3 Biochemical functionalization of NDs

BMP-2 derived peptide was grafted to as-received and dry-oxidized NDs using EDC/NHS-mediated crosslinking chemistry. Therefore 0.4 mg of EDC and 0.6 mg of NHS were successively added per 1 mL of ND suspension to a final concentration of 2 mM and 5 mM, respectively. The chemicals were allowed to react for 5 min at room temperature. Subsequently, 1.4 µL of 2-mercaptoethanol per 1 mL of ND suspension (final concentration 20 mM) were added to quench the EDC. The peptide was directly suspended into the NHS-activated ND suspensions to a final concentration of 100 µg/mL of peptide. The mixtures of NDs and peptide was incubated for 24 h at 700 rpm and 37 °C using the ThermoMixer® by Eppendorf AG,

Hamburg, Germany. Afterwards the ND suspensions were centrifuged for 30 min at 14000 g using the MiniSpin®-plus centrifuge by Eppendorf AG, Hamburg, Germany. The supernatants were collected to determine the amount of the peptide and the functionalized ND pellets were washed twice with ddH_2O.

2.3 Structural characterization

In order to determine the functional surface groups of NDs, Fourier-transform infrared spectroscopy (FT-IR) and inductively coupled plasma atomic emission spectroscopy (ICP-OES) were used. Infrared absorption spectra of NDs were recorded from 400 cm^{-1} to 4000 cm^{-1} with 32 scan cycles and resolution of 1 cm^{-1} using a Vertex 70 FTIR spectrometer from Bruker, Billerica, MA, USA in pellets with KBr (1:100 mass ratio of sample to KBr). ICP-OES was used to quantify the ND surfaces using the selective sodium ion exchange of $NaHCO_3$ to carboxylic acids. Therefore, 1.5 g NDs were mixed with 50 mL of 0.05 M $NaHCO_3$ according to the Boehm titration method [28]. The mixture was allowed to react at 40 °C for 24 h. Afterwards, centrifugation (4000 g for 30 min) was conducted using Allegra® X-15R centrifuge by Beckman Coulter Inc., Brea, CA, USA with a swinging-bucket rotor and 10 kDa Amicon® ultra centrifugal filters by Merck KGaA, Darmstadt, Germany. The sodium content of the initial and reacted $NaHCO_3$ was determined using the ICP-OES Optima 8300 by PerkinElmer Inc., Waltham, MA, USA. The device was operated by 1500 W at 40 MHz with 12 L/min plasma gas flow and calibrated using 1% HNO3.

Fluorescence spectroscopy was used to quantify the conjugated BMP-2 derived peptide. The instrument used for fluorescence emission measurements was a Fluoromax-4 spectrofluorometer by Horiba Ltd., Kyoto, Japan. The calibration was set using serial two-fold dilutions of 100 µg/mL aqueous peptide solution. The excitation wavelength was 274 nm and the emission was measured in the range of 290-350 nm with a slit opening of 5 nm and in increments of 0.5 nm.

Agglomerate size distribution and zeta potential measurements were obtained using Zetasizer Nano ZS by Malvern Panalytical GmbH, Kassel, Germany. Before the measurements, ND suspensions were homogenized for 5 min using ultrasonic cleaner by VWR International GmbH, Darmstadt, Germany. The folded polycarbonate capillary zeta cell (model: DTS1070) by Malvern Panalytical GmbH, Kassel, Germany with inbuilt gold plated copper electrodes was applied for agglomerate size and zeta potential measurements. Each measurement was repeated 3 times including an intermediate cleaning step of the cuvette with ethanol and ddH_2O.

3. Results and discussion

3.1 Surface quantification of oxidized NDs

Crosslinking techniques of amide and thiol compounds require deprotonated carbonyl compounds [29,30,31]. In order to enrich the ND surface with carbonyl containing surface groups, wet and dry oxidation pathways present promising approaches [32]. FT-IR measurements of various ND surface modifications were performed to determine the species of functional surface groups. Fig 1 compares the infrared spectra of the as-received, wet- and dry-oxidized functional ND surface groups.

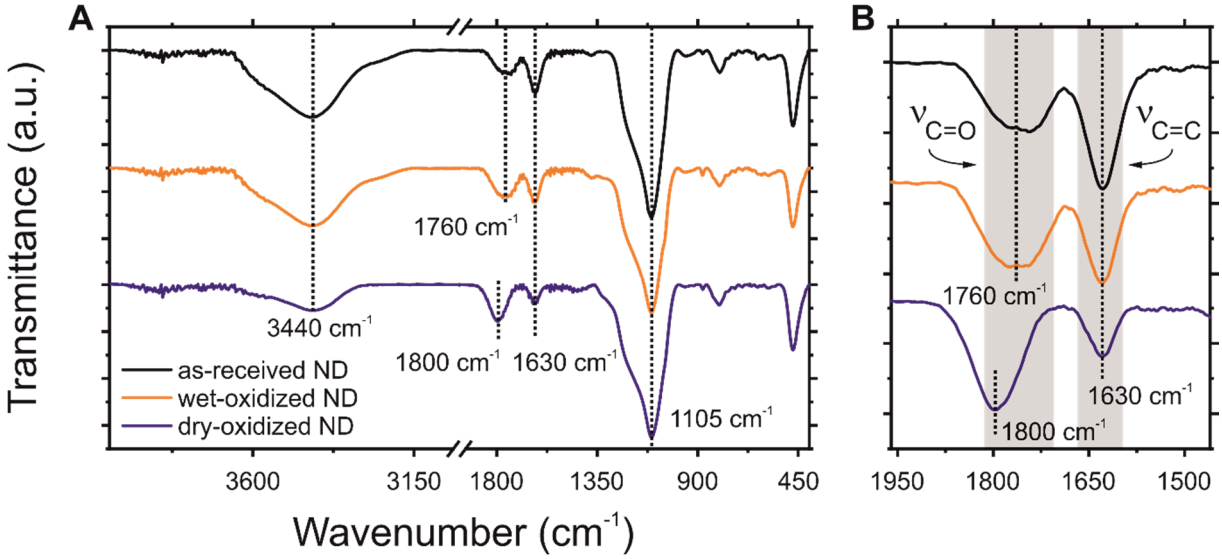

Fig. 1 (A) Infrared spectra of as-received (black), wet- (orange) and dry-oxidized (blue) NDs, (B) in the spectral range 1460-1960 cm^{-1}. Grey boxes indicate the stretch vibration of carbonyl ($\nu_{C=O}$) compounds in the range 1710-1810 cm^{-1} and sp^2 carbon ($\nu_{C=C}$) in the range 1600-1680 cm^{-1}, respectively.

As shown in Fig. 1 (A) all ND surface modifications possess the same stretch vibrations ν_{O-H} at 3660-3300 cm^{-1}, $\nu_{C=C}$ peak at 1630 cm^{-1} and ν_{C-O} peak at 1105 cm^{-1} [33,34]. The carbonyl stretch vibrations $\nu_{C=O}$ are expected at 1850-1710 cm^{-1}, whereby $\nu_{C=O}$ of acid anhydrides at 1800 cm^{-1} and $\nu_{C=O}$ of carboxylic acids at 1760 cm^{-1} are observed, respectively [35]. Fig. 1 (B) displays the FT-IR spectra in the range of 1460-1960 cm^{-1}. As shown in the grey boxes, the surface loading of carbonyl compounds (C=O) are increasing and sp^2 carbon compounds (C=C) are decreasing on the ND surface, due to the respective oxidation method. Whereby a high intensity (I) ratio of $I(\nu_{C=O})/I(\nu_{C=C})$ represents an absolute higher quantity of carbonyl compounds on the ND surface. The highest amount of carbonyl compounds was observed for the dry-oxidized NDs. The wet oxidation increased the amount of carboxylic acids, whereas

dry oxidation leads to the conversion into acid anhydrides on the ND surface. The conversion of functional ND surface groups into acid anhydrides is favourable in the absence of water and requires the dehydration of carboxylic acids. We can report the formation of acid anhydrides onto ND surface after air annealing at 415 °C for 5 h, while Sotoma *et al.* observed the acid anhydride formation at 600 °C for 5 h [36]. Dideikin *et al.* indicated a sp^3-sp^2 rehybridization of carbon atoms at 450 °C and annealing time of 1 h [37]. The conversion of functional ND surface groups into carbonyl compounds is strongly related to the initial sp^3/sp^2 carbon ratio, which depends on the actual manufacturer [38]. In order to compare the ND surface chemistry, the intensity ratio of $\nu_{C=O}$ and $\nu_{C=C}$ was calculated. Fig. 2 illustrates the quantitative comparison of as-received, wet- and dry-oxidized ND surfaces.

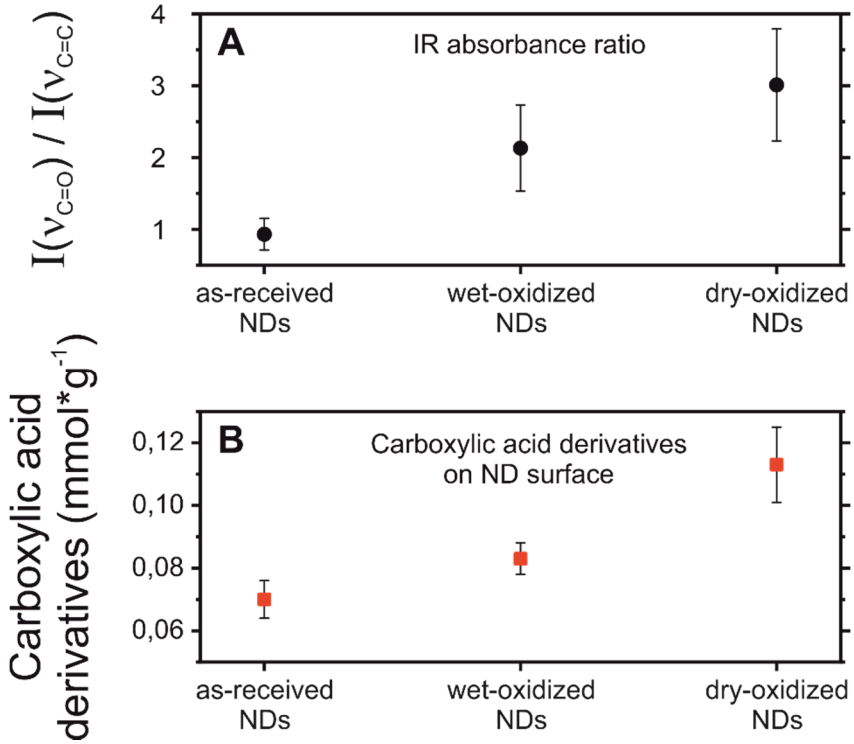

Fig. 2 Comparison of as-received, wet- and dry-oxidized ND surface modifications. Diagram (A) represents the infrared absorbance ratio of carbonyl ($\nu_{C=O}$) to sp^2 carbon ($\nu_{C=C}$) compounds and (B) surface loading of carboxylic acid derivatives onto ND surface obtained from ICP-OES.

As shown in Fig. 2 (A) the highest ratio of $I(\nu_{C=O})/I(\nu_{C=C})$ was obtained for dry-oxidized NDs. Wet-oxidized NDs have 2.3-fold while dry-oxidized NDs possess 3.2-fold from the amount of carbonyl compounds of as-received NDs. Therefore, the area underneath the respective peak of the infrared spectra has been evaluated and processed. In order to quantify the amount of carboxylic acid derivatives, mass spectroscopy was conducted. Fig. 2 (B) shows the amount of

carboxylic acid derivatives on the ND surface. As-received NDs exhibit 0.07±0.01 mmol/g, wet-oxidized NDs 0.083±0.01 mmol/g and dry-oxidized NDs 0.113±0.01 mmol/g of carboxylic acid derivatives. The specific dissociation of Na^+-ions of $NaHCO_3$ to carboxylic acids was used to determine the total surface loading onto NDs [39]. Despite the different surface carbonyl species, NDs with a high amount of acid anhydrides show the highest amount of Na^+-ions on their surface. Aqueous alkaline media are able to regenerate carboxylic acids from acid anhydrides [40]. Therefore, acid anhydrides will be hydrolysed to carboxylic acids which in turn act as compounds to bind for example biomolecules to the ND surface.

3.2 Dependence of ND surface modification on BMP-2 derived peptide loading efficiency

BMP-2 derived peptide was grafted to as-received and dry-oxidized NDs. The EDC/NHS-mediated amide formation was used to covalently bind the osteogenic peptide to the nanoscaled ND agglomerates [41]. In order to quantify the amount of the peptide grafted onto NDs, fluorescence spectroscopy was used. Fig. 3 shows the surface loading of NDs with the peptide and the correlated calibration curve. The amide formation was verified using infrared spectroscopy.

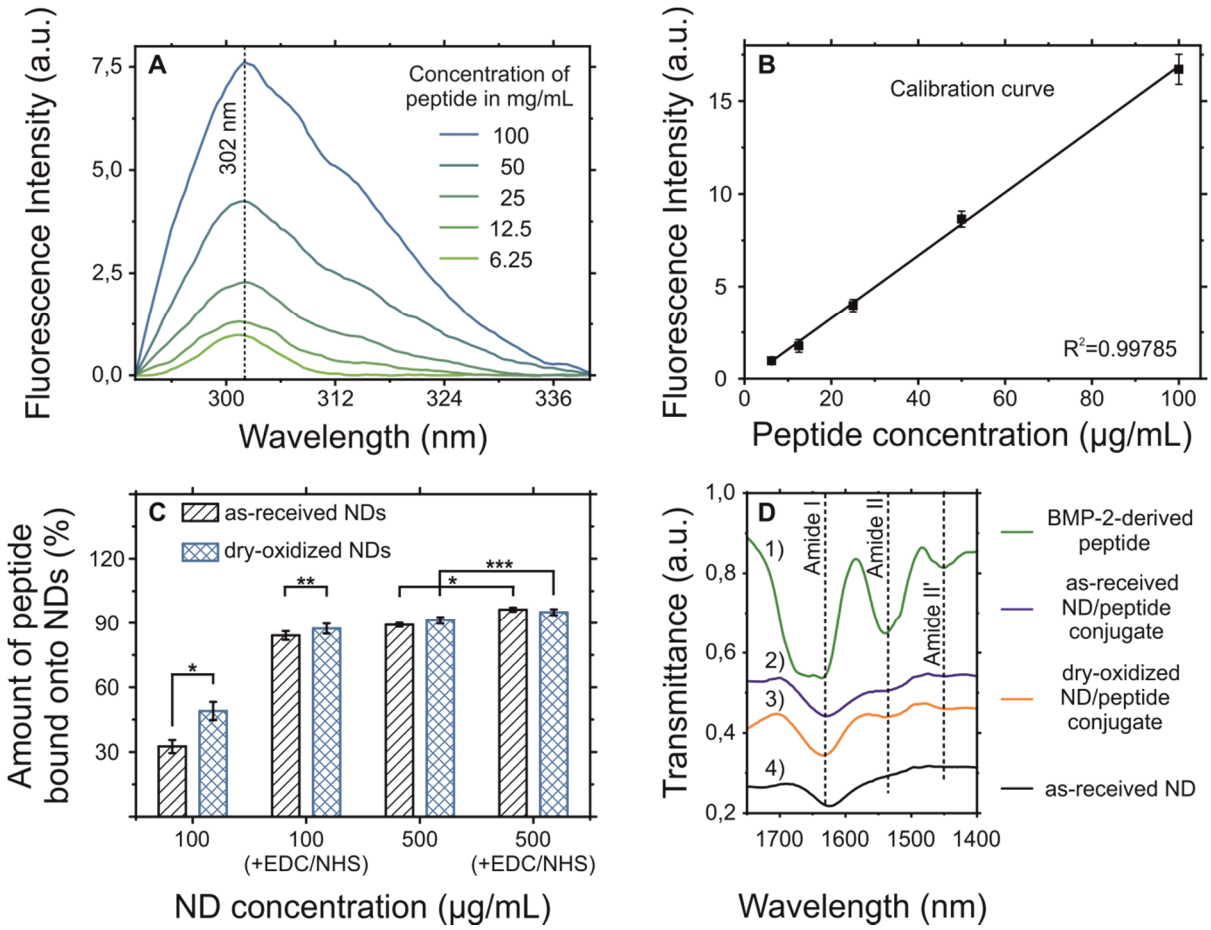

Fig. 3 (A) Fluorescence spectra for various BMP-2 derived peptide concentrations and (B) calibration curve (n = 3 and R^2 = 0.99785) of the fluorescence intensity as function of peptide concentration. (C) Amount of peptide in [%] bonded to 100 and 500 µg/mL of as-received and dry-oxidized NDs. Initial peptide concentration for conjugation $c_{peptide}$ = 100 µg/mL. n = 3; unpaired t-test * P < 0.01; ** P < 0.15; *** P < 0.05. (D) Infrared spectroscopy of 1) BMP-2 derived peptide, 2) as-received ND/peptide conjugate, 3) dry-oxidized ND/peptide conjugate and 4) as-received ND without peptide.

As shown in Fig. 3 (A), the integral autofluorescence intensity around 302 nm of the BMP-2 derived peptide was used to correlate its concentration. The fitted regression line in Fig. 3 (B) displays a high coefficient of determination with 99.785%, which refers to the little variability of the obtained data. The surface loading of NDs and the related quantity of BMP-2 derived peptide loaded onto their surface was calculated by subtracting the amount of the unbound peptide from the initial loading amount after conjugation. The amount of peptide was determined using fluorescence spectroscopy. Fig. 3 (C) indicates the surface loading efficiency of the peptide onto NDs, where 100 µg/mL of the peptide were loaded onto 100 µg/mL (1:1 ND-peptide) and 500 µg/mL (5:1 ND-peptide) of NDs, respectively. In general, the dry-oxidized NDs show a higher amount of peptide on their surface, although the difference to as-received NDs is not significant for high amount of tethered peptide. In case of the 1:1 ND-peptide ratio without EDC/NHS, the dry-oxidized NDs have an absolute surface loading efficacy of 49±4%, which is 17±2% higher compared to the as-received NDs. While with EDC/NHS activation the absolute surface loading of as-received NDs is 84±2% and dry-oxidized NDs 87±3%. Following the EDC/NHS-mediated conjugation the interaction of the peptide with NDs is based on chemisorption, wherein without EDC/NHS peptides are mainly adsorbed onto NDs. The significant higher amount of tethered peptide using EDC/NHS and the influence of different ND-peptide ratio was confirmed using unpaired t-tests. P-values below 0.05 indicating a relevant difference between the populations of NDs with and without EDC/NHS-mediated conjugation as well as among the respective oxidation technique for a significance level of 5%. Dry-oxidized NDs exhibit a higher surface loading compared to wet-oxidized NDs if the ND-peptide ratio is 1:1. As the ND-peptide ratio increases the surface loading onto NDs increases simultaneously starting from under 50% to over 80% of bonded peptide. If EDC/NHS was added to the system, the surface loading of NDs increases independently in respect to the employed ND-peptide ratio. The addition of EDC/NHS enables the possibility to control the surface loading even at low ND-peptide ratio and ensure the economical application of NDs. At surface loadings higher than 80% the discrepancy for as-received and dry-oxidized NDs is considered to be not statistically significant (P < 0.15). This

phenomena is related to the maximum surface loading for 1:1 ND-peptide mass ratio, since steric and hydration repulsion inhibit further peptides to approach the ND surface [42]. With an increased amount of NDs and ultimately covalent binding sites, the surface loading capability can be enhanced. In case of 5:1 ND-peptide ratio with EDC/NHS activation the absolute surface loading was slightly increased with 96±1% for as-received and 95±1% for dry-oxidized NDs. Fig. 3 (D) provides the evidence of the EDC/NHS-mediated amide formation between the BMP-2 derived peptide and NDs. The BMP-2 derived peptide (1) shows the typical infrared bands of amide I at 1630 cm^{-1}, amide II at 1540 cm^{-1} and amide II' at 1450 cm^{-1} [43,44]. Amide I vibration arises mainly from the stretch vibration $\nu_{C=O}$ and is visible in all samples (1-4), whereas amide II and amid II' are depicted in ND-peptide conjugates (2-3). The visible amide II (N-H) and amid II' (C-N) bands as well as the increased surface loading in case of the EDC/NHS-mediated amide formation, provide the evidence of covalent compounds between the BMP-2 derived peptide and NDs. In order to confirm the stability of the ND peptide binding, agglomerate size distribution and zeta potential measurements have been employed. As-received and dry-oxidized ND agglomerates with an initial mean hydrodynamic diameter of 26±2 nm and 34±5 nm at pH = 9 were used to bind the BMP-2 derived peptide. After EDC/NHS-mediated conjugation, as-received and dry-oxidized NDs show an increased mean agglomerate size distribution of 1020±143 nm (as-received NDs) and 100±4 nm (dry-oxidized NDs) with the correlated zeta potential of -11±1 mV and -33±1 mV, respectively. This increase of the agglomerate size is mainly attributed to re-aggregation of the NDs during the sedimentation process related to sample collection and centrifugation. Hence, as-received NDs are not stable after conjugation with the BMP-2 derived peptide at pH = 9 [45]. Concerning the high agglomerate size, further separation techniques of unbounded peptide and conjugated NDs such as cascade centrifugation and dialysis have to be considered [46,47]. Additional biocompatible dispersing agents and different crosslinking approaches are able to improve the outcome of the conjugation [48,49].

4. Conclusion

In summary, this report is the first describing the covalent surface loading of NDs using a cysteine-terminated BMP-2 derived peptide and the quantification of its loading efficacy. The employed ND agglomerate sizes for the conjugation were 26±2 nm for the as-received and 34±5 nm for the oxidized NDs, respectively. We have shown the feasibility of a controlled biomolecule loading onto NDs for drug delivery applications. The optimized loading of biomolecules onto NDs was done in the range of 33-96% total surface coverage using an

EDC/NHS-mediated amide formation. The applied carbodiimide crosslinker chemistry was suitable to covalently bind 96% of BMP-2 derived peptide at a given ND-peptide ratio of 5:1. Disadvantages of the EDC/NHS conjugation are the high pH sensitivity of the chemical reaction and its cytotoxicity at high concentrations. Concerning the translational relevance of the ND conjugates, further cytotoxicity tests have to be conducted systematically. Main advantages are the water solubility of EDC and NHS as well as the high selectivity to carboxylic acids. EDC/NHS conjugation can be conduct under physiological conditions to covalently graft biomolecules onto nanoparticles. Furthermore, excess crosslinking reagents can be removed using washing with ddH_2O. In order to promote the surface loading of NDs with the peptide, wet and dry oxidation of NDs was performed and evaluated using infrared and mass spectroscopy. It has been demonstrated, that dry-oxidized NDs show the highest amount of carboxylic acid derivatives with 0.113±0.012 mmol/g compared to wet-oxidized NDs with 0.083±0.005 mmol/g and as-received NDs with 0.07±0.006 mmol/g. The authors strongly recommend dry-oxidized NDs as initial surface modification for further physisorption or chemisorption of small biomolecules and drugs. Additional drug binding will be possible applying simultaneously conjugation of different species using the approach of the current study or further physisorption of drugs. This work will open the pathway to the development of the systematic understanding, and consequently optimization of NDs as drug delivery vehicles.

Acknowledgement

We gratefully acknowledge the support through the International Excellence Graduate School on Emerging Materials and Processes Korea (iEGSEMP Korea) in the context of TU Dresden's Institutional Strategy (ZUK 64), funded by the Excellence Initiative of the German Federal and State Governments. This research was supported under the “Mid-career Researcher Program” (NRF-2016R1A2B2014612) supervised by the NRF (National Research Foundation) in Republic of Korea.

References

[1] Mochalin VN, Shenderova O, Ho D, Gogotsi Y. The properties and applications of nanodiamonds. Nat Nanotechnol 2012;7:11-23.

[2] Zhang Y, Rhee KY, Hui D, Park SJ. A critical review of nanodiamond based nanocomposites: Synthesis, properties and applications. Compos B Eng 2018;143:19-27.

[3] Neburkova J, Vavra J, Cigler P. Coating nanodiamonds with biocompatible shells for applications in biology and medicine. Curr Opin Solid St M 2017;21:43-53.

[4] Cao N, Yang B, Barras A, Szunerits S, Boukherroub R. Polyurethane sponge functionalized with superhydrophobic nanodiamond particles for efficient oil/water separation. Chem Eng J 2017;307:319-325.

[5] Turcheniuk K, Mochalin VN. Biomedical applications of nandiamonds (Review). Nanotechnology 2017;28:1-27.

[6] Ho D, Wang CHK, Chow EKH. Nanodiamonds: The intersection of nanotechnology, drug development, and personalized medicine. Sci Adv 2015;1:1-14.

[7] Zhang W, Patel K, Schexnider A, Banu S, Radadia AD. Nanostructuring of Biosensing Electrodes with Nanodiamonds for Antibody Immobilization. ACS Nano 2014;8:1419-1428.

[8] Whitlow J, Pacelli S, Paul A. Multifunctional nanodiamonds in regenerative medicine: recent advances and future directions. J Control Release 2017;261:62-86.

[9] Panich AM, Salti M, Goren SD, Yudina EB, Aleksenskii AE, Ya Vul A. Gd(III)-Grafted Detonation Nanodiamonds for MRI Contrast Enhancement. J Phys Chem C 2019;123:2627-263.

[10] Lee DK, Kim SV, Limansubroto AN, Yen A1, Soundia A, Wang CY, et al. Nanodiamond-Gutta Percha Composite Biomaterials for Root Canal Therapy. ACS Nano 2015;9:11490-11501.

[11] Lim DG, Rajasekaran N, Lee D, Kim NA, Jung HS, Hong S, et al. Polyamidoamine-Decorated Nanodiamonds as a Hybrid Gene Delivery Vector and siRNA Structural Characterization at the Charged Interfaces. ACS Appl Mater Interfaces 2017;9:31543-31556.

[12] Chan MS, Liu LS, Leung HM, Lo PK. Cancer-Cell-Specific Mitochondria-Targeted Drug Delivery by Dual-Ligand-Functionalized Nanodiamonds Circumvent Drug Resistance. ACS Appl Mater Interfaces 2017;9:11780-11789.

[13] Pacelli S, Maloney R, Chakravarti AR, Whitlow J, Basu S, Modaresi S, et al. Controlling Adult Stem Cell Behavior Using Nanodiamond-Reinforced Hydrogel: Implication in Bone Regeneration Therapy. Sci Rep 2017;7:1-15.

[14] Wang Z, Wang Z, Lu WW, Zhen W, Yang D, Peng S. Novel biomaterial strategies for controlled growth factor delivery for biomedical applications. NPG Asia Mater 2017;9:1-17.

[15] Moore L, Gatica M, Kim H, Osawa E, Ho D. Multi-protein Delivery by Nanodiamonds Promotes Bone Formation. J Dent Res 2013;92:976-981.

[16] Li D, Chen X, Gong Y, Zhang B, Liu Y, Jin P, et al. Synthesis and Vacuum Cold Spray Deposition of Biofunctionalized Nanodiamond/Hydroxyapatite Nanocomposite for Biomedical Applications. Adv Eng Mater 2017;19:1-6.

[17] Hustedt JW, Blizzard DJ. The Controversy Surrounding Bone Morphogenetic Proteins in the Spine: A Review of Current Research. Yale J Biol Med 2014;87:549-561.

[18] James AW, LaChaud G, Shen J, Asatrian G, Nguyen V, Zhang X, et al. A Review of the Clinical Side Effects of Bone Morphogenetic Protein-2. Tissue Eng Part B Rev 2016;22:284-297.

[19] Wang MH, Zhou XM, Zhang MY, Shi L, Xiao RW, Zeng LS, et al. BMP2 promotes proliferation and invasion of nasopharyngeal carcinoma cells via mTORC1 pathway. Aging (Albany NY) 2017;9:1326-1339.
[20] Carragee EJ, Chu G, Rohatgi R, Hurwitz EL, Weiner BK, Yoon ST, et al. Cancer Risk After Use of Recombinant Bone Morphogenetic Protein-2 for Spinal Arthrodesis. J Bone Joint Surg Am. 2013;95:1537-1545.
[21] Lo KWH, Ulery BD, Ashe KM, Laurencin CT. Studies of Bone Morphogenetic Protein based Surgical Repair. Adv Drug Deliv Rev 2012;64:1277-1291.
[22] El Bialy I, Jiskoot W, Nejadnik MR. Formulation, Delivery and Stability of Bone Morphogenetic Proteins for Effective Bone Regeneration. Pharm Res 2017;34:1152-1170.
[23] Luo Z, Yang Y, Deng Y, Sun Y, Yang H, Wei S. Peptide-incorporated 3D porous alginate scaffolds with enhanced osteogenesis for bone tissue engineering. Colloids Surf B Biointerfaces 2016;143:243-251.
[24] Gaillard C, Girard HA, Falck C, Paget V, Simic V, Ugolin N et al. Peptide nucleic acid–nanodiamonds: covalent and stable conjugates for DNA targeting. RSC Adv 2014; 4:3566.
[25] Zheng WW, Hsieh YH, Chiu YC, Cai SJ, Cheng CL, Chen C. Organic functionalization of ultradispersed nanodiamond: synthesis and applications. J. Mater. Chem. 2009;19:8432-8441.
[26] Saito A, Suzuki Y, Ogata S, Ohtsuki C, Tanihara M. Activation of osteo-progenitor cells by a novel synthetic peptide derived from the bone morphogenetic protein-2 knuckle epitope. Biochim Biophys Acta 2003;1651:60-67.
[27] Jee AY, Lee M. Surface functionalization and physicochemical characterization of diamond nanoparticles. J Appl Phys 2009;9:144-147.
[28] Goertzen SL, Thériault KD, Oickle AM, Tarasuk AC, Andreas HA. Standardization of the Boehm titration. Part I. CO2 expulsion and endpoint determination. Carbon 2010;48:1252-1261.
[29] Lake MP, Bouchard LS. Targeted nanodiamonds for identification of subcellular protein assemblies in mammalian cells. PLoS One 2017;12:1-18.
[30] Iimura S, Manabe K, Kobayashi S. Direct thioesterification from carboxylic acids and thiols catalyzed by a Brønsted acid. Chem Commun 2002:94-95.
[31] Hermanson GT. Bioconjugate Techniques. 3rd Ed. London:Elsevier;2013.
[32] Krüger A, Lang D. Functionality is Key: Recent Progress in the Surface Modification of Nanodiamond. Adv Funct Mater 2012;22:890-906.
[33] Song P, Yu Y, Wu Q, Fu S. Facile fabrication of HDPE-g-MA/nanodiamond nanocomposites via one-step reactive blending. Nanoscale Res Lett 2012;7:355-342.
[34] Gonçalves JPL, Shaikh AQ, Reitzig M, Kovalenko DA, Michael J, Beutner R, et al. Detonation nanodiamonds biofunctionalization and immobilization to titanium alloy surfaces as first steps towards medical application. Beilstein J Org Chem 2014;10: 2765-2773.
[35] Chung PH, Perevedentseva E, Tu JS, Chang CC, Cheng CL. Spectroscopic study of bio-functionalized nanodiamonds. Diam Relat Mater 2006;15:622-625.
[36] Sotoma S, Akagi K, Hosokawa S, Igarashi R, Tochio H, Harada Y et al. Comprehensive and quantitative analysis for controlling the physical/chemical states and particle properties of nanodiamonds for biological applications. RSC Adv. 2015;5:13818.
[37] Dideikin AT, Aleksenskii AE, Baidakova MV, Brunkov PN, Brzhezinskaya M, Davydov VY. Rehybridization of carbon on facets of detonation diamond nanocrystals and forming hydrosols of individual particles. Carbon 2017;122:737:745.

[38] Osswald S, Yushin G, Mochalin V, Kucheyev SO, Gogotsi Y. Control of sp2/sp3 Carbon Ratio and Surface Chemistry of Nanodiamond Powders by Selective Oxidation in Air. J Am Chem Soc 2006;128:11635-11642.
[39] Schmidlin L, Pichot V, Comet M, Josset S, Rabu P, Spitzer D. Identification, quantification and modification of detonation nanodiamond functional groups. Diam Relat Mater 2012;22:113-117.
[40] Gold V. The hydrolysis of acetic anhydride. J Chem Soc Faraday Trans 1948;44:506-518.
[41] Liu YL, Sun KW. Protein Functionalized Nanodiamond Arrays. Nanoscale Res Lett 2010;5:1045-1050.
[42] Guerrini L, Alvarez-Puebla RA, Pazos-Perez N. Surface Modifications of Nanoparticles for Stability in Biological Fluids. Materials 2018;11:1154.
[43] Kong J, Yu S. Fourier transform infrared spectroscopic analysis of protein secondary structures. Acta Biochim Biophys Sin 2007;39:549-59.
[44] Barth A. Infrared spectroscopy of proteins. Biochim Biophys Acta 2007;1767:1073-101.
[45] Gibson N, Shenderova O, Luo TJM, Moseenkov S, Bondar V, Puzyr A et al. Colloidal stability of modified nanodiamond particles. Diam Relat Mater 2009;18:620-626.
[46] Backes C, Hanlon D, Szydlowska BM, Harvey A, Smith RJ, Higgins TM et al. Preparation of Liquid-exfoliated Transition Metal Dichalcogenide Nanosheets with Controlled Size and Thickness: A State of the Art Protocol. J Vis Exp 2016; 118:e54806.
[47] Zhou Y, He C, Chen K, Ni J, Cai Y, Guo X et al. A New Method for Evaluating Actual Drug Release Kinetics of Nanoparticles inside Dialysis Devices via Numerical Deconvolution. J Control Release 2016;243:11-20.
[48] Studart AR, Amstad E, Gauckler LJ. Colloidal Stabilization of Nanoparticles in Concentrated Suspensions. Langmuir 2007;23:1081-1090.
[49] Moore CJ, Montón H, O'Kennedy R, Williams DE, Nogués C, Crean C et al. Controlling colloidal stability of silica nanoparticles during bioconjugation reactions with proteins and improving their longer-term stability, handling and storage. J Mater Chem B 2015;3:2043.